ACS Catalysis

Research Article

pubs.acs.org/acscatalysis

Rate-Determining Step in the NO_x Reduction Mechanism on BaY Zeolites and the Importance of Long-Range Lattice Effects

Xiaoying Bao, Chun-Yi Sung, Randall Q. Snurr,* and Linda J. Broadbelt*

Department of Chemical and Biological Engineering and Institute for Catalysis in Energy Processes, Northwestern University, Evanston, Illinois 60208, United States

Supporting Information

ABSTRACT: The mechanism of the NO_x reduction reaction on BaNaY zeolite using acetic acid/acetate as a reductant has been explored using density functional theory. The elementary steps, the reaction intermediates, and the transition states were identified on a zeolite cluster consisting of 10 tetrahedral atoms (10T). The hydrogen abstraction reaction of acetic acid/acetate was identified as the rate-determining elementary step at 473 K. The long-range electrostatic effect of the lattice on the rate-determining step was studied on expanded 24T, 30T, 34T, 40T, 44T, and 50T zeolite clusters. It was found that while acetate may be greatly stabilized on the expanded clusters with additional Na^+ cations and Al atoms, the stabilization of acetic acid is much less affected by the long-range lattice effect. The reaction barrier of the hydrogen abstraction reaction, on the other hand, is less sensitive to the long-range lattice effect. The results of this paper highlight the importance of long-range electrostatic effects on the modeling of "single-site" catalysts involving ionic species.

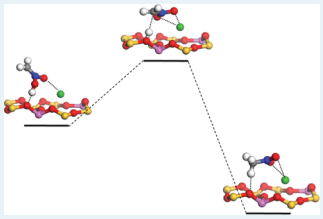

KEYWORDS: *NOx reduction, zeolite, barium, quantum chemistry, reaction mechanism, long-range effects*

INTRODUCTION

Reduction of NO_x is a pressing issue in the area of environmental catalysis because of strict regulations on the emission of NO_x from automobiles in many countries.[1,2] Zeolites are a family of microporous, crystalline structures that are able to host different cations for various applications as heterogeneous catalysts,[3,4] and the potential of zeolites for the selective catalytic reduction (SCR) of nitrogen oxides (NO_x) to nitrogen under excess oxygen conditions, such as lean-burn and diesel engines, has attracted much attention. Among the many zeolite-based catalysts that have been studied for the SCR of NO_x,[5−14] BaNaY is particularly interesting since it has been reported that acetaldehyde or acetic acid, which is formed from hydrocarbons in a nonthermal plasma, reduces NO_x to N_2 over BaNaY catalysts at a relatively low temperature (473 K), with a high NO_x conversion (>90%) and a high resistance to water vapor.[15−18]

Sachtler, Weitz, and co-workers used FTIR and isotopic labeling techniques to probe the chemistry of the deNO_x reactions in BaNaY. A number of intermediates were identified, and a reaction mechanism for the formation of N_2 from the reaction of acetaldehyde or acetic acid with NO_2 and NO was proposed.[19−21] The proposed overall mechanism involves the following steps: (**A**) the formation of NH_3 from the reaction of acetaldehyde or acetic acid with NO_2; (**B**) the formation of HNO_2 from the reaction between water and the NO_x species; (**C**) the reaction between ammonia and HNO_2, which forms ammonium nitrite (NH_4NO_2) that can swiftly decompose into N_2 and H_2O.[22] Furthermore, the formation of nitromethane (CH_3NO_2), an important intermediate in step **A**, was identified as the rate-determining reaction(s) from experiments, since NO_x reduction to N_2 proceeds with a high rate and a high nitrogen yield at 413 K when nitromethane is used as the primary reductant.[23] The successive reactions for the formation of nitromethane from the reaction of acetate ion with NO_2 were proposed as follows:[23]

$$CH_3CO_2^-{}_{(ads)} + NO_2 \Leftrightarrow \cdot CH_2CO_2^-{}_{(ads)} + HNO_2 \quad (1)$$

$$\cdot CH_2CO_2^-{}_{(ads)} + NO_2 \Leftrightarrow O_2NCH_2CO_2^-{}_{(ads)} \quad (2)$$

$$O_2NCH_2CO_2^-{}_{(ads)} \Leftrightarrow CO_2 + \cdot CH_2NO_2^-{}_{(ads)} \quad (3)$$

$$\cdot CH_2NO_2^-{}_{(ads)} + H^+_{(ads)} \Leftrightarrow CH_3NO_{2(ads)} \quad (4)$$

Note that $CH_3CO_2^-$, $\cdot CH_2CO_2^-$, $O_2NCH_2CO_2^-$, and $\cdot CH_2NO_2^-$ are in equilibrium with their neutral parent molecules, CH_3COOH, CH_2COOH, O_2NCH_2COOH, and $\cdot CH_2NO_2H$, respectively. Yeom et al.[23] indicated that the hydrogen abstraction from $CH_3COOH/CH_3CO_2^-$ may be facilitated by NO_2 (See reaction 1). However, information about the reaction mechanism at the atomic level, such as the structural relationship between the intermediates and the catalyst, was not provided by experiments.

In our previous studies, the adsorption properties of the above intermediates and the characteristics of the dissociative adsorption were investigated to unravel the effect of the local environment of the zeolite using a quantum mechanics/molecular mechanics (QM/MM) methodology with a 10T QM cluster.[24,25] It was found that the adsorbates, except for HNO_3,

Received: October 10, 2011
Revised: January 25, 2012
Published: January 30, 2012

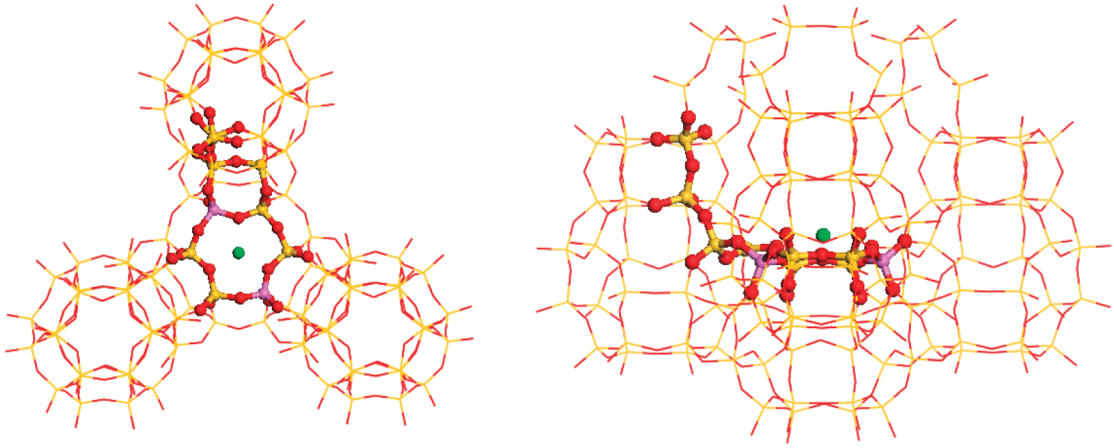

Figure 1. Two different views of the 10T cluster (ball and stick representation) embedded in a super cage of faujasite zeolite (wire and frame representation). One Ba^{2+} ion is located at the center of an S6R (Site II). Two Al atoms are in the para location on the S6R, denoted as (1,4). In the figure: O (red), Si (yellow), Al (pink), Ba (green).

are more stabilized in their neutral form than their dissociated form on the 10T zeolite cluster. In the present work, the same 10T cluster is used to understand how the neutral and dissociated intermediates in the proposed rate-determining reaction(s) shown in reactions 1 to 4 transform using ab initio calculations.[26−32] The rate-determining reaction on the 10T cluster was probed. Furthermore, expanded 24T, 34T, 40T, 44T, and 50T QM clusters were constructed to understand the long-range electrostatic effect of the lattice on the reaction pathway.

COMPUTATIONAL METHODS

Experimental studies have shown that the Ba^{2+} cations in BaNaY zeolites are the most active sites for NO_2 reduction.[19,33−35] Site II, located at the center of a single six-membered ring (S6R) in the super cages of zeolite Y, is the most favorable site for Ba^{2+} coordination.[35] To study the deNO_x reactions on BaNaY zeolite, a 10T cluster including one S6R and four more tetrahedral atoms extended from the S6R was constructed as described in our earlier work.[25] Figure 1 shows the 10T cluster in a super cage of zeolite Y. The outermost Si and O atoms of the 10T cluster were saturated with hydrogen atoms directed along the bond vector of what would have been the next zeolite framework atom in the crystal structure. The Si−H and O−H distances were fixed at 1.49 and 0.96 Å, respectively. Both the outermost Si and O atoms and the capping hydrogen atoms were fixed at their crystallographic positions. All other atoms including barium, atoms in the adsorbates, and other framework atoms in the 10T cluster were allowed to relax. Similar termination/relaxation schemes were employed for the expanded 24−50 T clusters.

Two aluminum atoms are needed for the cluster to be charge neutral when one Ba^{2+} ion is included. The locations of the aluminum atoms are limited by Löwenstein's rule,[36] which states that two aluminum-centered tetrahedra cannot share an oxygen atom. High-resolution ^{29}Si and ^{27}Al MAS NMR studies have shown that in Y zeolite, the hexagonal S6R may contain two Al either in the para or in the meta location.[37−39] None of the S6R rings contains three Al atoms, and some may include only one Al atom.[37−39] According to our previous work,[25] a (1,4) Al arrangement shown in Figure 1 is able to stabilize the Ba^{2+} cation well, while the Al arrangements with only one Al in the S6R are not able to stabilize the Ba^{2+} as well. Therefore, the reaction pathways were studied using a 10T cluster with the (1,4) Al arrangement.

The electronic energies of the intermediates and transition states on the 10T cluster were calculated with density functional theory (DFT). The B3LYP functional was used to describe the electron exchange and correlation. The 10T cluster was treated with a mixed basis set SDD:6-31G(d,p):6-311++G(d,p).[40] Namely, the SDD effective-core potential was used to describe the Ba atom. The 6-311++G(d,p) basis set was used to describe the sorbate molecule and the framework atoms near the sorbate atoms to effectively describe the hydrogen bonding between the negatively charged framework oxygen atoms and the sorbate molecule. The 6-31G(d,p) basis set was used to describe all other atoms. The detailed assignment of basis sets for individual atoms can be found in the Supporting Information, Figure S1. This combination of functional and basis set was chosen based on calculations on barium-containing molecules summarized in our previous study and the reduction in computational cost offered by the smaller basis set on atoms belonging to the framework farther from the active site,[24] and it was implemented by using the GEN keyword in Gaussian 03.[41] All of the structures investigated in the present study are most stable in their lowest spin state.

To find the reaction intermediates and transition states, multiple initial configurations were used for each optimization. The energetics of the reaction intermediates and transition states were then evaluated based on their Gibbs free energies at 473 K using standard statistical mechanical formulas within the rigid rotor, harmonic oscillator approximation as follows:[42]

$$H = E_0 + E_{ZPE} + E_v + E_t + E_r + RT \quad (5)$$

$$S = S_v + S_t + S_r \quad (6)$$

$$G = H - TS \quad (7)$$

where H, E, S, and G denote enthalpy, internal energy, entropy, and Gibbs free energy, respectively. Subscripts "0", "ZPE", "v", "t", and "r" denote contributions from electronic energy, zero-point energy, vibration, translation, and rotation, respectively. R is the gas constant, and T is the temperature.

In the frequency calculations, imaginary vibrational modes due to the artificially fixed atoms of the clusters were removed by the level-shift technique[43] as in our previous studies.[24] The level-shift technique shifts the vibrational modes corresponding

dx.doi.org/10.1021/cs200519p | ACS Catal. 2012, 2, 350−359

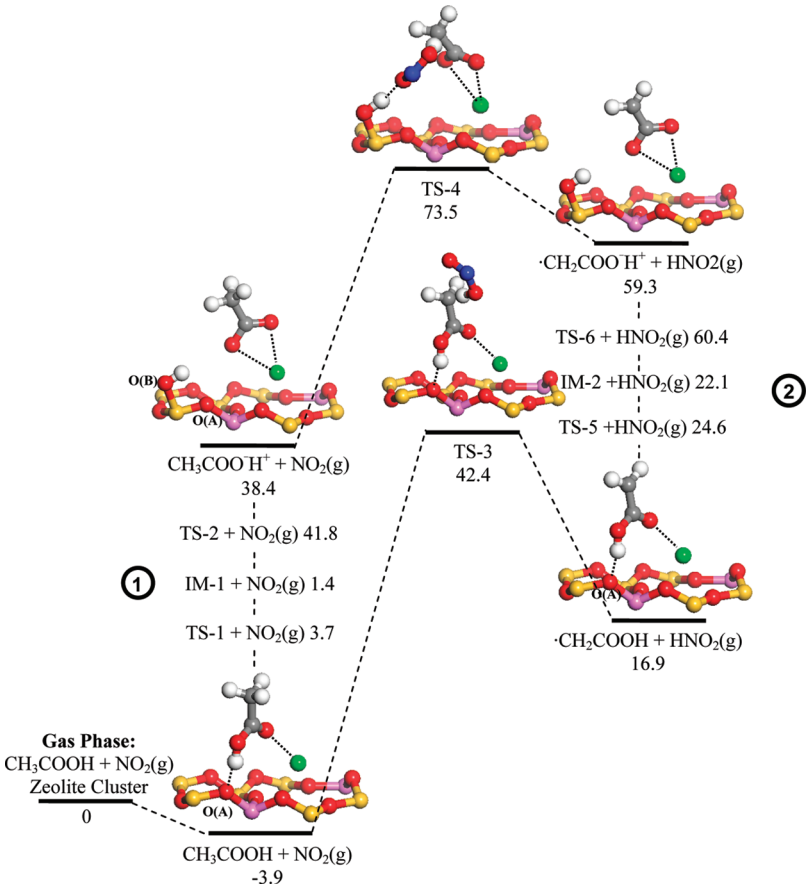

Figure 2. Calculated energy profile for reaction step (1) on the 10T cluster. IM and TS stand for intermediate and transition state, respectively. Only selected IMs and TSs are shown; the geometries of all other IMs and TSs can be found in the Supporting Information, Figure S2. For the geometries, only the sorbate molecules and a part of the 10T cluster are shown. The numbers are BSSE-corrected Gibbs free energies in kcal/mol. In the Figure: O (red), Si (yellow), Al (pink), Ba (green), H (white), C (gray), N (blue).

to the vibrations of the fixed atoms to very large wave numbers, which are then discarded.[43] Minima were confirmed by no imaginary frequencies after the level-shift procedure. Transition states were confirmed by the presence of one and only one imaginary frequency after the level-shift procedure. To confirm that the transition states are connected to the correct energy minima, the transition states were perturbed slightly along the reaction coordinate in the directions of the reactant and the product. The perturbed geometries were used as starting points for energy minimizations which eventually led to the associated energy minima. Gibbs free energy values were calculated within the rigid rotor, harmonic oscillator approximation using the level-shifted frequencies. No scale factor was available for the particular combination of functional and basis set that we employed, so the frequencies were used unscaled. Basis set superposition error (BSSE) corrections using the counterpoise method[44] were taken into account. All calculations were carried out using the Gaussian 03 software.[41]

RESULTS AND DISCUSSION

Reaction Pathway on the 10T Cluster. In this section, reactions 1−4 will be discussed sequentially on the 10T cluster with the (1,4) Al arrangement shown in Figure 1. It is to be noted that for ease of comparison between different species, the electronic and free energies of adsorption, ΔE_{ads} and ΔG_{ads}, in this paper are defined with respect to the 0 energy reference state which consists of a zeolite cluster, a CH_3COOH molecule, and a NO_2 molecule separated infinitely apart in vacuum (see Figure 2).

Figure 2 shows the calculated energy profiles for the adsorption of CH_3COOH and the subsequent reaction step (1), together with the geometries of selected reaction intermediates and transition states. The geometries of all other intermediates and transition states can be found in the Supporting Information, Figure S2. For a clearer presentation, only part of the zeolite cluster is shown. The adsorption of CH_3COOH has a large electronic adsorption energy (ΔE_{ads}) of −26.2 kcal/mol and a much smaller Gibbs free energy of adsorption (ΔG_{ads}) of −3.9 kcal/mol because of the entropy loss during adsorption. For adsorbed CH_3COOH, one of its O atoms of the carboxyl group is coordinated to the Ba^{2+} cation, while the H atom in the hydroxyl group is coordinated to a framework O atom, O(A) (See Figure 2).

On the 10T cluster, the dissociated $CH_3COO^-H^+$ has a positive ΔE_{ads} of 18.8 kcal/mol and a ΔG_{ads} of 38.4 kcal/mol. The H atom of the dissociated $CH_3COO^-H^+$ molecule is bonded to a framework O atom, O(B), at an OH bond distance of 0.98 Å.

An NO_2 molecule can perform a hydrogen abstraction from either CH_3COOH or $CH_3COO^-H^+$ (see TS-3 and TS-4 in Figure 2). In this step, one of the oxygen atoms in the NO_2 molecule obtains a hydrogen atom from the methyl group of the adsorbed CH_3COOH or $CH_3COO^-H^+$, producing an adsorbed $\cdot CH_2COOH$ or $\cdot CH_2COO^-H^+$ molecule and a gas-

dx.doi.org/10.1021/cs200519p | ACS Catal. 2012, 2, 350−359

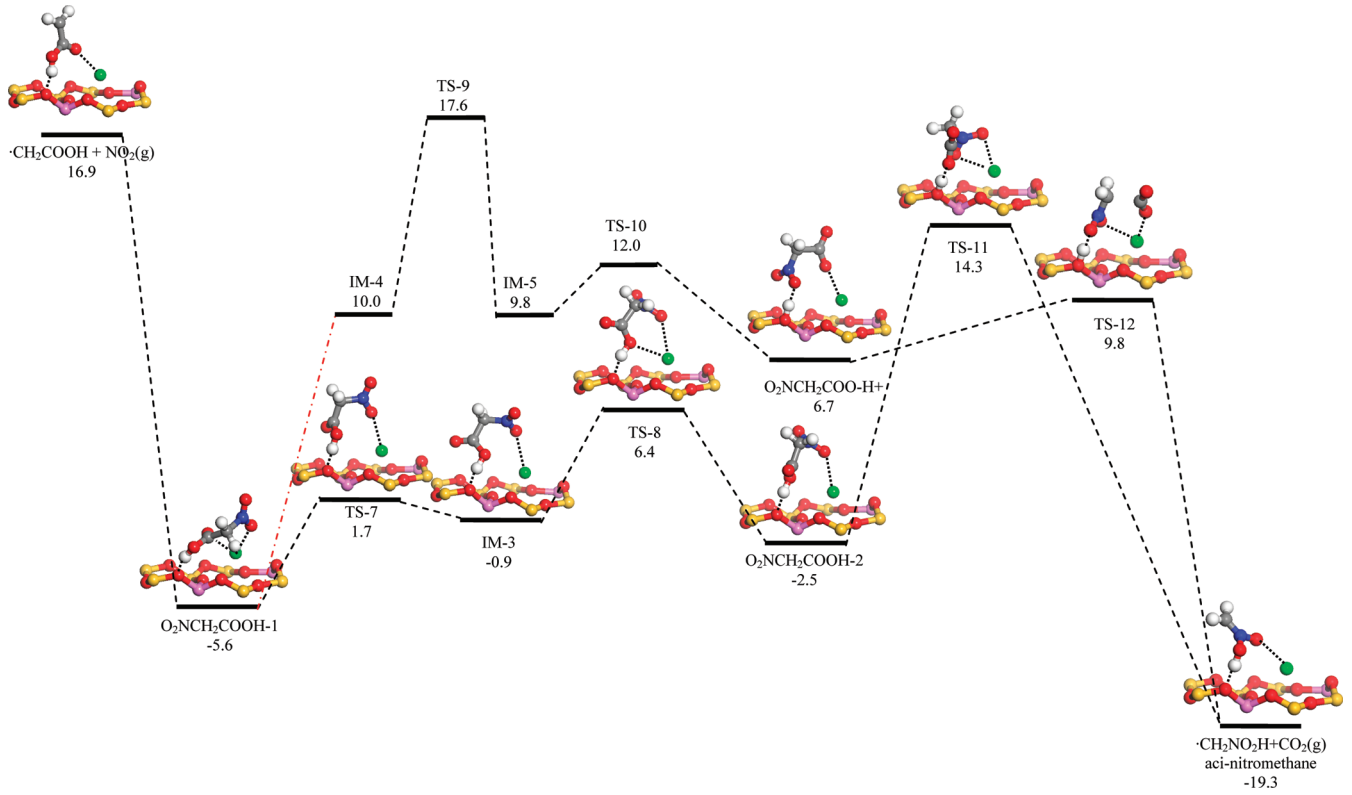

Figure 3. Calculated free energy profile for reactions 2 and 3 on the 10T cluster. IM and TS stand for intermediate and transition state, respectively. Only selected IMs and TSs are shown; the geometries of all other IMs and TSs can be found in the Supporting Information, Figure S2. For the geometries, only the sorbate molecules and a part of the 10T cluster are shown. The numbers are BSSE-corrected Gibbs free energies in kcal/mol. In the figure: O (red), Si (yellow), Al (pink), Ba (green), H (white), C (gray), N (blue). The path marked by the red dash-dot line was not fully explored.

phase HNO_2 molecule. When CH_3COOH is the reactant, the Gibbs free energy barrier $\Delta G^{\ddagger}$ for the hydrogen abstraction reaction is 46.3 kcal/mol, which is a result of both the large loss of entropy occurring upon adsorption of an NO_2 molecule and the large endothermicity of the reaction. For example, the entropic contribution to the free energy barrier at 473 K is 18.6 kcal/mol while the enthalpic contribution is 27.6 kcal/mol. On the other hand, hydrogen abstraction from $CH_3COO^-H^+$ has a free energy barrier $\Delta G^{\ddagger}$ of 35.1 kcal/mol, more than 10 kcal/mol less endergonic than that for CH_3COOH. This is due to the stabilization of the NO_2 molecule by the dissociated proton atom when $CH_3COO^-H^+$ is the reactant (see TS-4 in Figure 2).

The product of the hydrogen abstraction reaction, either adsorbed $\cdot CH_2COOH$ or $\cdot CH_2COO^-H^+$, has a very similar configuration to that of either adsorbed CH_3COOH or $CH_3COO^-H^+$, respectively, and they can interconvert, as shown by path ② in Figure 2. The details of path ② are very similar to path ① and are shown in Supporting Information, Figure S2.

Figure 3 shows the calculated energy profiles for the reactions 2 and 3, the NO_2 addition reaction and the CO_2 elimination reaction. In step (2), a gas phase NO_2 molecule reacts with the $\cdot CH_2COOH$ radical to form an O_2NCH_2COOH molecule (named as O_2NCH_2COOH-1). This reaction proceeds without an energy barrier and has a favorable free energy change of −22.5 kcal/mol.

O_2NCH_2COOH-1 rearranges by interacting with the zeolite framework atoms to either O_2NCH_2COOH-2 (neutral route) or $O_2NCH2COO^-H^+$ (ionic route). Reaction 3, the CO_2 elimination reaction, may proceed either via O_2NCH_2COOH-2 or $O_2NCH2COO^-H^+$ to form the product $\cdot CH_2NO_2H$. In the neutral route, the highest free energy barrier of 16.8 kcal/mol along the reaction landscape suggests that the transformation from O_2NCH_2COOH-2 to the products is the rate-limiting step. However, the overall free energy required to rearrange O_2NCH_2COOH-1 to O_2NCH_2COOH-2 must also be taken into account, as O_2NCH_2COOH-2 is uphill on the free energy surface from O_2NCH_2COOH-1, which is required for the formation of O_2NCH_2COOH-2. If the energy barriers along the route to convert O_2NCH_2COOH-1 to O_2NCH_2COOH-2 are low, as they are in this case, then O_2NCH_2COOH-1 and O_2NCH_2COOH-2 can be assumed to be in quasi-equilibrium, thereby resulting in a net free energy barrier, $\Delta G^{\ddagger}$, for the overall conversion from O_2NCH_2COOH-1 to $\cdot CH_2NO_2H$ equal to 19.9 kcal/mol (i.e., (−2.5 − (−5.6) = 3.1 kcal/mol; 3.1 + 16.8 = 19.9 kcal/mol). In the ionic route, not all transition states and intermediates from O_2NCH_2COOH-1 to $O_2NCH_2COO^-H^+$ have been located (marked by the red dash-dot line in Figure 3). However, judging from those that were successfully located (IM-4, TS-9, IM-5, TS-10), it is seen that on the 10T cluster, large energy barriers of at least 23.2 kcal/mol need to be crossed to form $\cdot CH_2NO_2H$ from O_2NCH_2COOH-1 via $O_2NCH2COO^-H^+$.

Therefore, on the 10T cluster, the formation of $\cdot CH_2NO_2H$ from O_2NCH_2COOH-1 via O_2NCH_2COOH-2 would dominate. Nonetheless, on the expanded clusters that will be discussed in the following sections, it is possible that the ionic species present during the transition from O_2NCH_2COOH-1 to $O_2NCH_2COO^-H^+$ (IM-4, IM-5, TS-9, TS-10) are better

dx.doi.org/10.1021/cs200519p | ACS Catal. 2012, 2, 350−359

stabilized, hence making the ionic route competitive with the neutral route.

Figure 4 shows the calculated energy profile of reaction 4, namely, the intramolecular H transfer reaction which isomerizes

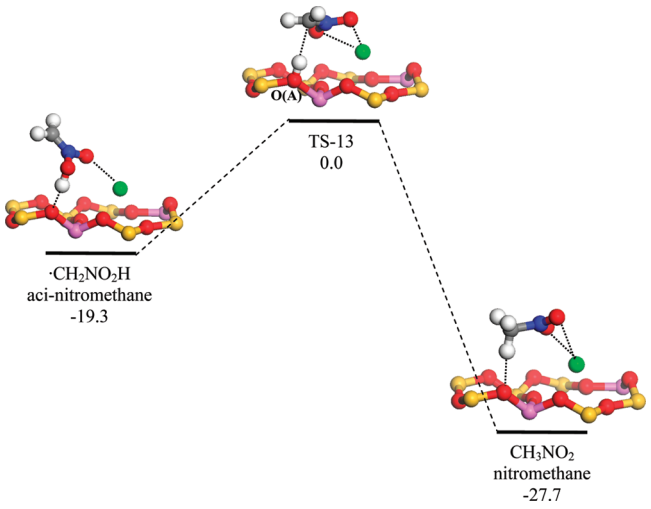

Figure 4. Calculated energy profile for reaction step (4). Only the sorbate molecules and a part of the 10T cluster are shown. The numbers are BSSE-corrected Gibbs free energies in kcal/mol. IM and TS stand for intermediate and transition state, respectively. In the figure: O (red), Si (yellow), Al (pink), Ba (green), H (white), C (gray), N (blue).

aci-nitromethane ($\cdot CH_2NO_2H$) into nitromethane (CH_3NO_2). From the structure of TS-13, it is seen that this step is significantly facilitated by the framework oxygen atom O(A). The free energy of adsorption of aci-anion nitromethane $\cdot CH_2NO_2^-$ is 16.7 kcal/mol (shown in Supporting Information, Figure S2), which is 35.9 kcal/mol higher than that of $\cdot CH_2NO_2H$. Therefore, the route from $\cdot CH_2NO_2^-$ to CH_3NO_2 is not further explored. However, it is possible that $\cdot CH_2NO_2^-$ may be further stabilized on the expanded clusters discussed in the following sections.

Long-Range Effect of the Lattice on the Stabilization of CH_3COOH and $CH_3COO^-H^+$. From the above discussions, it is seen that on the 10T cluster, the hydrogen abstraction step has the largest Gibbs free energy barrier, and it is the rate-determining elementary step of the overall reaction. The Gibbs free energy barrier of the hydrogen abstraction reaction is large (46.3 kcal/mol) if CH_3COOH is the reactant, while it is smaller (35.1 kcal/mol) if $CH_3COO^-H^+$ is the reactant. On the other hand, while the adsorption of CH_3COOH on the 10T cluster is favorable, the adsorption of $CH_3COO^-H^+$ is unfavorable. In other words, the reaction is difficult regardless of whether CH_3COOH or $CH_3COO^-H^+$ is the starting species.

Several studies have shown that the long-range effect of the lattice is an important factor to consider to accurately describe reactions in zeolites.[29,45−48] In the case of BaNaY, the Ba^{2+} active sites are surrounded by other Ba^{2+} and Na^+ cations. Therefore, it is important to understand the effect of these additional cations on the reaction intermediates and reaction barriers.

To rationally expand the 10T cluster, it is important to examine the local environment around the Ba^{2+} active site. The molecular formula of BaNaY that was studied experimentally by Yeom et al. for the NO_x reduction[19] is $Ba_{9.6}Na_{33.8}Al_{53}Si_{139}O_{384}{*}xH_2O$. In a unit cell of BaNaY, there are 32 Site IIs and 16 Site Is shared by 8 super cages. On average, each super cage contains one Ba^{2+} cation (9.6/8 ≈ 1). Site II and Site I are the most and second most favorable binding sites for Ba^{2+} and Na^+. IR spectroscopy of adsorbed CO and CO_2[34] and single-crystal X-ray diffraction techniques[33] showed that almost all of the 9.6 Ba^{2+} cations are located at Site II. Consequently, the 33.8 Na^+ have to bind with the remaining 22.4 (32−9.6) Site IIs and 16 site Is. In other words, while all of the Site IIs are filled with either Ba^{2+} or Na^+, the Site Is are not completely filled, 11.4 (33.8−22.4) Na^+ cations will have to be located at the 16 Site Is in each unit cell.

To illustrate, Figure 5 shows a top-down view of a super cage where the Ba^{2+}-occupied Site II (single 6-membered ring, S6R)

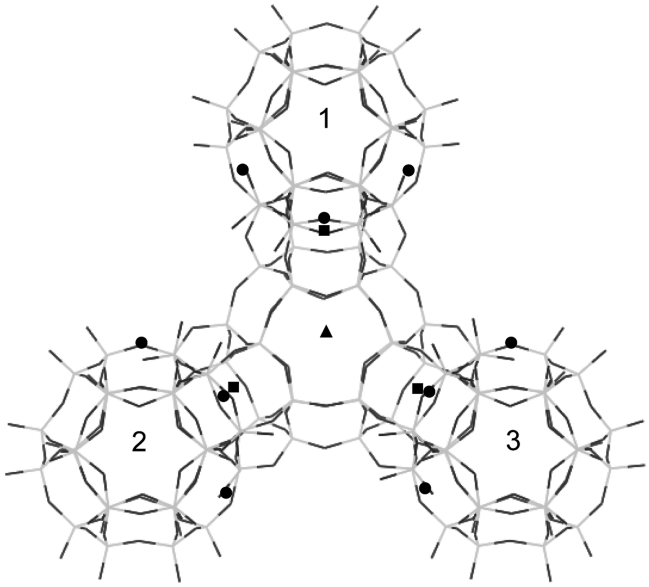

Figure 5. Schematic illustration of the Ba^{2+} active site and the nearby cation sites. In the figure: O (dark gray), Si (light gray), Ba^{2+}-occupied Site II (filled triangle ▲), Na^+-occupied Site II (filled circle ●), Site I that may or may not be occupied by Na^+ (filled square ■).

is marked by a filled triangle (▲). Three identical branches of framework atoms, marked by 1, 2, and 3, extend from the Ba^{2+}-occupied Site II, forming a super cage. There are altogether nine Site IIs (●) and three Site Is (double 6-membered ring, D6R, ■) close to the Ba^{2+}-occupied Site II. It is assumed that these nine Site IIs are all occupied by a Na^+ cation, since the Ba^{2+} cations would assume maximum distances between each other to minimize repulsion. On the other hand, the three Site Is may or may not be occupied by a Na^+ cation. Therefore, it is necessary to study situations where zero, one, two, or three of the Site Is are occupied by Na^+ cations.

On the basis of the above discussions, the 10T cluster was expanded to a 24T cluster with one Ba^{2+} located at a Site II, three nearby Na^+ cations in Site II, and zero Na^+ cations in Site I as shown in Figure 6. (Results with one, two, or three Na^+ cations in Site I are discussed below.) Five Al atoms must be present in the 24T cluster to balance the positive charges of the three Na^+ and one Ba^{2+} cations. The Al atoms were placed according to the following guidelines. First, two out of the five Al atoms were placed in the S6R occupied by the Ba^{2+} cation to stabilize Ba^{2+}, according to our previous result.[25] Second, no Si(4Al) was allowed since the Si/Al ratio of the BaNaY zeolite

dx.doi.org/10.1021/cs200519p | ACS Catal. 2012, 2, 350−359

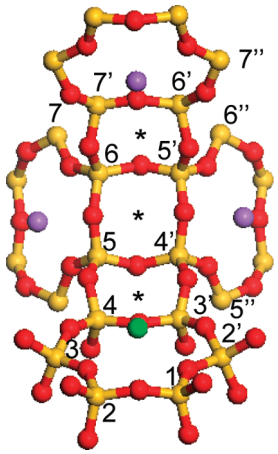

Figure 6. 24T cluster with the Ba^{2+} and Na^{+} cations located at the Site II positions (single 6-membered rings S6Rs). The three single 4-membered rings (S4Rs) are marked by asterisks. Five Al arrangements shown in Table 1 were investigated. In the figure: O (red), Si (yellow), Ba (green), Na (violet).

that was studied experimentally[19] is 2.67, which means the possibility of any Si(4Al) is extremely low.[49,50] Third, Lowenstein's rule was obeyed. Following these guidelines, five different Al arrangements shown in Table 1 (24T-I to 24T-V)

Table 1. Gibbs Free Energies of Adsorption of CH_3COOH and $CH_3COO^-H^+$ on the 24T Clusters with Various Al Arrangements (B3LYP/SDD)[a]

name	Al arrangement	CH_3COOH ΔG_{ads} (kcal/mol)	$CH_3COO^-H^+$ ΔG_{ads} (kcal/mol)
24T-I	2′, 4, 6, 6′, 6″	−12.1	−12.4
24T-II	2′, 4, 5′, 7′, 7″	−10.3	−9.7
24T-III	2′, 4, 4′, 6, 6′	−9.2	−8.0
24T-IV	2′, 3, 4′, 6, 6′	−6.8	1.0
24T-V	2′, 3, 5″, 6′, 7	−2.8	10.0

[a]The arrangements of the five Al atoms are indicated by five numbers which refer to the positions of the Al atoms in Figure 6.

were investigated. The main difference between these five Al arrangements is the arrangement of Al on the three single 4-membered rings (S4Rs, marked by asterisks in Figure 6), whose atoms are closest to the sorbate molecules. For example, for 24T-I to 24T-V, there are 3, 3, 4, 3, and 1 Al atoms on the three S4Rs, respectively. In other words, 24T-I to 24T-IV have a higher Al density on the three S4Rs than 24T-V. It is to be noted that the experimentally measured energies are averages over various Al arrangements in the zeolite sample used. However, instead of trying to make direct comparison with experimental values, here we investigate how local environment can affect the energetics.

To search for the energy minima of CH_3COOH/$CH_3COO^-H^+$ on a given 24T cluster, a number of different initial configurations were attempted for the quantum chemical energy optimizations. The initial configurations were chosen based on the following three criteria: First, at least one oxygen atom from the carboxyl group of the CH_3COOH/$CH_3COO^-H^+$ molecule is interacting with the Ba^{2+} cation. This is to be consistent with the experimental observation that Ba^{2+} is the main active site. Second, the other O atom in the carboxyl group of $CH_3COO^-H^+$ may be interacting closely with the strongly positively charged Ba^{2+}, Na^{+}, or the dissociated proton. Third, the H atom attached to the carboxyl group of CH_3COOH or the dissociated proton from $CH_3COO^-H^+$ is interacting with a framework O atom. This is to make sure that the positively charged H atom or the proton is stabilized by the negative charge of the framework O atom.

The use of a mixed basis set SDD:6-31G(d,p):6-311++G(d,p), as described in the methods section, on the expanded cluster is difficult because of the large computational time required. Instead, an all SDD basis set was used to treat the 24T cluster and all other expanded clusters described hereafter. To validate the use of the all SDD basis set, key reaction intermediates and transition states shown in Figure 2 were recalculated using the all SDD basis set and are shown in Supporting Information, Figure S3. Table 2 compares key

Table 2. Comparison of the Gibbs Free Energies of Adsorption and Reaction Barriers of Key Intermediates and Reactions Calculated by Using the Mixed Basis Set and the All SDD Basis Set

Gibbs free energies of adsorption (kcal/mol)			reaction barriers for the hydrogen abstraction reaction (kcal/mol)		
	mixed basis set	all SDD basis set		mixed basis set	all SDD basis set
CH_3COOH	−3.9	−10.8	from CH_3COOH	46.3	41.3
$CH_3COO^-H^+$	38.4	41.7	from $CH_3COO^-H^+$	35.1	24.9
$\cdot CH_2COOH$	59.3	53.4			
$\cdot CH_2COO^-H^+$	16.9	15.7			

adsorption energies and reaction barriers calculated by using the mixed basis set and the all SDD basis set. Qualitative agreement between the results from the mixed basis set and the all SDD basis set is seen. Comparison between Figure 2 and Supporting Information, Figure S3 also shows that the configurations of the reaction intermediates and transition states calculated using the mixed basis set and the all SDD basis set are very similar.

Table 1 shows the Gibbs free energies of adsorption for CH_3COOH and $CH_3COO^-H^+$ on the 24T clusters with five different Al arrangements. It is seen in Table 1 that 24T-I affords the best stabilization of both CH_3COOH and $CH_3COO^-H^+$, and the Gibbs free energy of adsorption for the two species are essentially identical (−12.4 and −12.1 kcal/mol). The minimum energy configurations of CH_3COOH and $CH_3COO^-H^+$ are shown in Figure 7. While one of the O atoms in the carboxylic group of the $CH_3COO^-H^+$ species is stabilized by the positively charged Ba^{2+} cation, the other O atom in the carboxylic group is best stabilized by the Na^{+} cation in one of the Site II positions. The attractive interaction between the Na^{+} cation and the O atom is so strong that it is able to move the Na^{+} out of its original position in Site II.

Table 1 also shows that the Al arrangements with more Al atoms in the three S4Rs (24T-I to 24T-IV) are able to stabilize both CH_3COOH and $CH_3COO^-H^+$ better than the Al arrangement with fewer Al atoms in the three S4Rs (24T-V). This may be attributed to the negative charges created by the Al atoms on the S4Rs. The negative charges help the stabilization of the positively charged H atoms in both CH_3COOH and $CH_3COO^-H^+$. In Table 1, it is also seen that the stabilization of

dx.doi.org/10.1021/cs200519p | ACS Catal. 2012, 2, 350−359

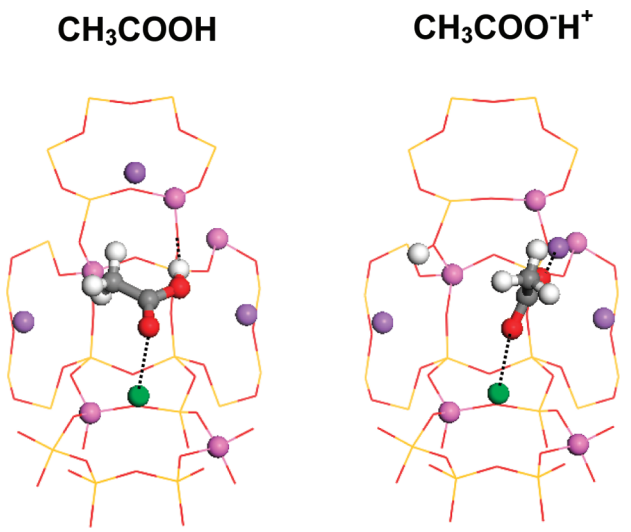

Figure 7. Minimum energy configurations of CH_3COOH and $CH_3COO^-H^+$ found on the 24T-I cluster. The sorbate molecule, the cations, and the Al atoms in the framework are shown in the ball and stick representation; all other atoms are shown in the wire and frame representation. $CH_3COO^-H^+$ is stabilized by one of the Na^+ cations. In the figure: O (red), Si (yellow), Na (violet), Ba (green), H (white), C (gray), Al (pink).

$CH_3COO^-H^+$ is much more sensitive to the Al arrangement than CH_3COOH. For example, the Gibbs free energies of adsorption of CH_3COOH on the five 24T clusters range from −12.1 to −2.8 kcal/mol, while the Gibbs free energies of adsorption of $CH_3COO^-H^+$ range from −12.4 to 10.0 kcal/mol.

It is interesting, however, to see that although all of the clusters from 24T-I to IV have high Al densities on the three S4Rs, some are able to stabilize both CH_3COOH and $CH_3COO^-H^+$ better than the others. To understand this, Figure 8 shows the minimum energy configurations of

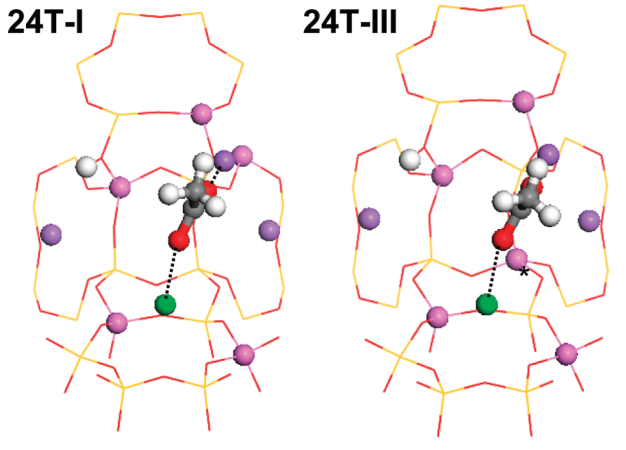

Figure 8. Minimum energy configurations of $CH_3COO^-H^+$ found on 24T-I and 24-III. The sorbate molecule, the cations, and the Al atoms in the framework are shown in the ball and stick representation, and all other atoms are shown in the wire and frame representation. In 24T-III, the Al atom marked by an asterisk creates a negative charge which repels the negatively charged oxygen atoms in the acetate. In the figure: O (red), Si (yellow), Na (violet), Ba (green), H (white), C (gray), Al (pink).

$CH_3COO^-H^+$ on 24T-I and 24T-III. A comparison shows that in 24T-III, there is an Al atom (marked by *) which creates a negative charge and repels the negatively charged O atoms in the carboxyl group. Clearly, certain arrangements of the Al atoms are able to create opposite dipoles to the CH_3COOH and $CH_3COO^-H^+$ molecules and hence help to stabilize these molecules.

The above discussion shows that compared with the 10T cluster, the 24T cluster is able to improve the stabilization of the ionic $CH_3COO^-H^+$ species drastically, which is mainly because the O atoms in the carboxyl group of $CH_3COO^-H^+$ can be stabilized by the Na^+ cations that are not present in the 10T cluster.

The 24T cluster was further expanded to 30T and 34T clusters to study the effect of a single Na^+-occupied Site I on the stabilization of CH_3COOH and $CH_3COO^-H^+$. Figure 9

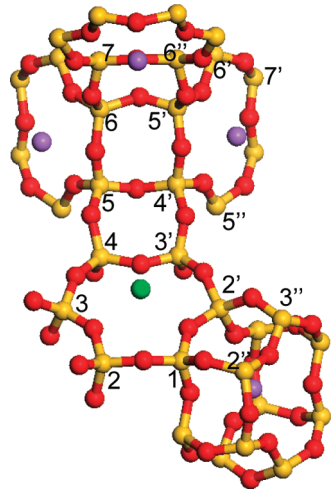

Figure 9. 34T cluster with one Ba^{2+} and three Na^+ cations located at the Site II positions (single 6-membered rings), and one Na^+ cation located at a Site I position (double 6-membered rings) opposite to the three Site IIs. Five Al arrangements shown in Table 3 were investigated. In the figure: O (red), Si (yellow), Na (violet), Ba (green).

shows the 34T cluster with a single Na^+-occupied Site I located opposite to the Na^+-occupied Site II positions. Five Al arrangements, 34T-I to 34T-V, were studied. Similar Al placement guidelines and minimum energy search protocols to the ones used for the 24T clusters were employed on the 34T clusters. The details of the five Al arrangements are listed in Table 3.

Table 3. Gibbs Free Adsorption Energies of CH_3COOH and $CH_3COO^-H^+$ on the 34T Clusters with Various Al Arrangements (B3LYP/SDD)[a]

name	Al arrangement	CH_3COOH ΔG_{ads} (kcal/mol)	$CH_3COO^-H^+$ ΔG_{ads} (kcal/mol)
34T-I	2′, 4, 5″, 6, 6′, 6″	−25.7	−30.1
34T-II	2′, 4, 4′, 6, 6″, 7′	−19.3	−25.2
34T-III	2, 2′, 4′, 6, 6″, 7′	−13.2	−12.2
34T-IV	3, 3′, 3″, 5, 5′, 7	−13.3	0.3
34T-V	2′, 2″, 4, 6, 6″, 7′	−10.0	0.5

[a]The arrangements of the five Al atoms are indicated by six numbers which refer to the positions of the Al atoms in Figure 9.

dx.doi.org/10.1021/cs200519p | ACS Catal. 2012, 2, 350–359

Table 3 shows the minimum adsorption free energies of CH_3COOH and $CH_3COO^-H^+$ on the 34T clusters with five different Al arrangements. It is seen that the CH_3COOH and $CH_3COO^-H^+$ species are best stabilized on 34T-I, which has an identical Al arrangement as 24T-I except for the additional Na^+-occupied Site I and the accompanying Al. Similar to what was observed on the 24T clusters, the stabilization of $CH_3COO^-H^+$ on the 34T clusters is more sensitive to the Al arrangement than that of CH_3COOH. For example, in Table 3, the highest and the lowest adsorption free energies of CH_3COOH are −25.7 and −10.0 kcal/mol, whereas the highest and the lowest adsorption free energies of $CH_3COO^-H^+$ are −30.1 and 0.5 kcal/mol. The additional Na^+-occupied Site I is able to further stabilize $CH_3COO^-H^+$ compared to CH_3COOH. For example, on 34T-I, the adsorption free energy of $CH_3COO^-H^+$ is −30.1 kcal/mol, which is about 4 kcal/mol lower than the adsorption free energy of CH_3COOH (−25.7 kcal/mol). In addition, the stabilization of CH_3COOH and $CH_3COO^-H^+$ is also sensitive to the position of the Na^+-occupied Site I. For example, the 30T cluster shown in Figure 10 has the same number of Al atoms and Na atoms as 34T-I, but the position of the additional Na^+-occupied Site I is different. Nonetheless, the ΔG_{ads} values of CH_3COOH and $CH_3COO^-H^+$ located on 30T are only −12.1 and −13.3 kcal/mol, respectively.

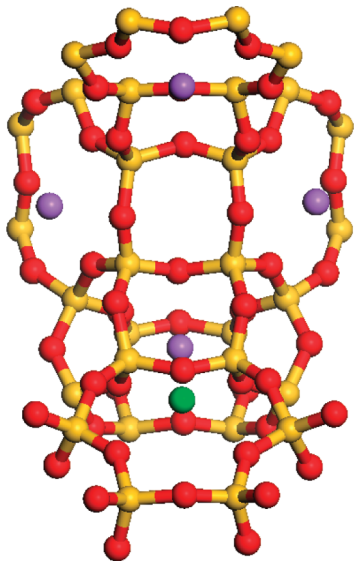

Figure 10. 30T cluster with one Ba^{2+} and three Na^+ cations located at the Site II positions (single 6-membered rings) and one Na^+ cation located at a Site I (double 6-membered ring) that is on the same side as the three Site IIs. In the figure: O (red), Si (yellow), Na (violet), Ba (green).

So far, the effect of zero or one Na^+-occupied Site I on the stabilization of CH_3COOH and $CH_3COO^-H^+$ has been discussed. To examine the effect of two or three Na^+-occupied Site I positions, cluster 34T-I was further expanded to a 40T and a 44T cluster with two Na^+-occupied Site I positions, and a 50T cluster with three Na^+-occupied Site I positions (see Supporting Information, Figure S4). Al arrangements similar to 34T-I were maintained on clusters 40T, 44T, and 50T. The Gibbs free energies of adsorption for both CH_3COOH and $CH_3COO^-H^+$ on the 40T, 44T, and 50T clusters are listed in Table 4. It is seen that adsorption of $CH_3COO^-H^+$ is preferred over adsorption of the neutral molecule CH_3COOH in all cases shown in Table 4, similar to the stabilization for 34T-I (Table 3). In addition, the minimum energy configurations of CH_3COOH and $CH_3COO^-H^+$ on these clusters are very similar to the ones on 34T-I, which suggests that further expansion of the zeolite cluster may not change the energetics of the reaction intermediates or transition states.

Table 4. Gibbs Free Adsorption Energies of CH_3COOH and $CH_3COO^-H^+$ on the 40T, 44T, and 50T Clusters with Al Arrangements Similar to That of 34T-I (B3LYP/SDD)[a]

	CH_3COOH ΔG_{ads} (kcal/mol)	$CH_3COO^-H^+$ ΔG_{ads} (kcal/mol)
34T-I	−25.7	−30.1
40T	−25.3	−30.9
44T	−21.2	−30.8
50T	−25.1	−26.2

[a]The details of the 40T, 44T, and 50T clusters are shown in Supporting Information, Figure S4.

Long-Range Lattice Effect on the Stabilization of Transition States. So far, the long-range lattice effect on the stabilization of CH_3COOH and $CH_3COO^-H^+$ has been discussed using expanded 24T, 30T, 34T, 40T, 44T, and 50T clusters. On the representative 24T and 34T clusters, five Al arrangements have been investigated. It is seen that the stabilization of the ionic species $CH_3COO^-H^+$ is much more sensitive to Al arrangement and cluster size than the neutral species CH_3COOH. For example, on the 10T cluster, the adsorption free energy of $CH_3COO^-H^+$ is much higher than that of CH_3COOH (41.7 vs −10.8 kJ/mol, SDD), whereas on the expanded clusters such as the 50 T cluster, the adsorption free energy of $CH_3COO^-H^+$ is similar to that of CH_3COOH (−26.2 vs −25.1 kJ/mol, SDD) It is to be noted, however, that only a limited number of Al arrangements were studied in this work because of high computational costs. Therefore, it is not our intent to conclude definitively that $CH_3COO^-H^+$ is more stable than CH_3COOH on BaNaY zeolite.

On the 10T cluster, the hydrogen abstraction reaction was identified as the rate-determining step of the overall reaction. To understand the long-range lattice effect on the hydrogen abstraction reaction barrier, the energy profile for this reaction was explored on one of the representative expanded clusters, the 34T-I cluster, and is shown in Figure 11.

Figure 11 shows that on cluster 34T-I, CH_3COOH converts to $CH_3COO^-H^+$ before the hydrogen abstraction reaction takes place. Interestingly, unlike the stabilization of the ionic species $CH_3COO^-H^+$, the free energy barrier of the hydrogen abstraction reaction is much less sensitive to the long-range electrostatic effect of the lattice. For example, the Gibbs free energy barrier of the hydrogen abstraction on cluster 34T-I is 29.8 kcal/mol, which is comparable to the free energy barrier of the same reaction on the 10T cluster (24.9 kcal/mol, see Table 2).

CONCLUSION

In this work, DFT calculations were performed on a 10T BaNaY zeolite cluster to probe the rate-determining step(s) of the NOx reduction reaction using acetic acid/acetate as a reductant. The calculations were performed using both a B3LYP/mixed basis set scheme and a computationally less costly B3LYP/SDD scheme. Qualitative agreement was obtained between the two schemes. On the 10T cluster, it was found that acetic acid is much better stabilized than acetate.

dx.doi.org/10.1021/cs200519p | ACS Catal. 2012, 2, 350−359

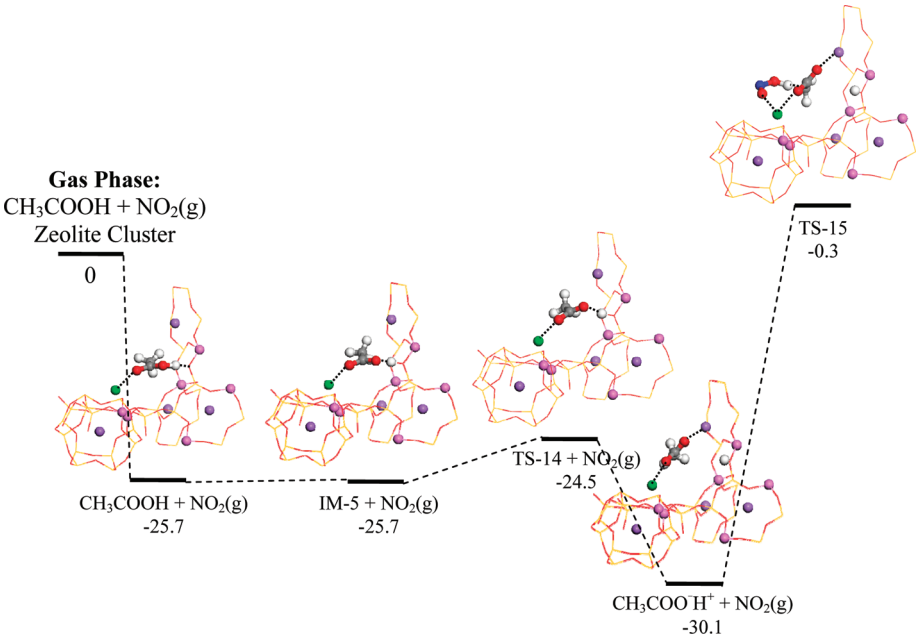

Figure 11. Calculated energy profile for reaction step (1) on the 34T-I cluster. The sorbate molecule, the cations, and the Al atoms in the framework are shown in the ball and stick representation, and all other atoms are shown in the wire and frame representation. IM and TS stand for intermediate and transition state, respectively. The numbers are BSSE-corrected Gibbs free energies in kcal/mol. In the figure: O (red), Si (yellow), Na (violet), Ba (green), H (white), C (gray).

For example, the Gibbs free adsorption energy of acetic acid is −3.9 kcal/mol (mixed basis set) or −10.8 kcal/mol (SDD), while the energy gap between the adsorbed acetic acid and its ionized adsorbed form is 42.3 kcal/mol (mixed basis set) or 52.5 kcal/mol (SDD). The hydrogen abstraction reaction from acetic acid was identified as the rate-determining elementary step at 473 K. The free energy barrier of this reaction with acetic acid as a reactant is 46.3 kcal/mol (mixed basis set) or 41.3 kcal/mol (SDD).

Expanded 24T, 30T, 34T, 40T, 44T, and 50T clusters were constructed to understand the long-range electrostatic effects of the lattice on the stabilization of the reaction intermediates and transition states. The calculations on the expanded clusters were done by using the computationally less costly B3LYP/SDD scheme. It was found that the stabilization of acetate may be greatly improved on the expanded clusters with additional Na^+ cations and Al atoms. On the other hand, the stabilization of acetic acid is much less affected by the long-range lattice effect. For example, on a 34T cluster, the Gibbs free energy of adsorption for acetic acid is −25.7 kcal/mol versus −10.8 on the 10T cluster, while the Gibbs free energy of adsorption for acetate is −30.1 kcal/mol versus +41.7 on the 10T cluster. The reaction barrier of the rate-determining elementary step, on the other hand, is less sensitive to the long-range lattice effect: the free energy barrier of the hydrogen abstraction reaction on the 34T cluster was found to be 29.9 kcal/mol (SDD), which is only about 5 kcal/mol higher than on the 10T cluster.

The results in this work provide an interesting case study about the importance of long-range electrostatic effects in zeolites and the quest for "single-site" catalysts. A Ba^{2+} cation in a single six-membered ring of a Y zeolite cavity may seem like a perfect single-site catalyst, but these results indicate that the locations of the surrounding cations can play an important role in stabilizing reaction intermediates and transition states, particularly for ionic species. Given the multitude of possible locations of these surrounding cations, the task of modeling catalysis on these sites is perhaps much more challenging than has been appreciated in the literature.

■ ASSOCIATED CONTENT

Supporting Information

The Supporting Information includes (1) the 10T cluster and its basis set assignment; (2) geometries of the intermediates and transition states that were not shown in the main text; (3) the geometries of the intermediates and transition states shown in Figure 2, recalculated using the all SDD basis set; and (4) the 40T, 44T and 50T clusters. This material is available free of charge via the Internet at http://pubs.acs.org.

■ AUTHOR INFORMATION

Corresponding Author

*E-mail: snurr@northwestern.edu (R.Q.S.), broadbelt@northwestern.edu (L.J.B.).

Funding

This work was supported by the Chemical Sciences, Geosciences, and Biosciences Division, Office of Basic Energy Sciences, Office of Science, U.S. Department of Energy Grant DE-FG-02-03ER15457. This research used resources of the National Energy Research Scientific Computing Center, which is supported by the Office of Science of the U.S. Department of Energy.

Notes

The authors declare no competing financial interest.

■ REFERENCES

(1) Klingstedt, F.; Arve, K.; Eranen, K.; Murzin, D. Y. *Acc. Chem. Res.* **2006**, *39*, 273−282.
(2) Twigg, M. V. *Appl. Catal., B* **2007**, *70*, 2−15.
(3) Breck, D. W. *Zeolite Molecular Sieves: Structure, Chemistry, and Use*; Wiley: New York, 1974.
(4) Weitkamp, J.; Puppe, L. *Catalysis and Zeolites: Fundamentals and Applications*; Springer: New York, 1999.

(5) Shelef, M. *Chem. Rev.* **1995**, *95*, 209−225.
(6) Campa, M. C.; Pietrogiacomi, D.; Tuti, S.; Ferraris, G.; Indovina, V. *Appl. Catal., B* **1998**, *18*, 151−162.
(7) Armor, J. N. *Catal. Today* **1995**, *26*, 147−158.
(8) Amiridis, M. D.; Zhang, T. J.; Farrauto, R. J. *Appl. Catal., B* **1996**, *10*, 203−227.
(9) Tabata, T.; Kokitsu, M.; Okada, O. *Catal. Lett.* **1994**, *25*, 393−400.
(10) Oleksenko, L. P.; Yatsimirsky, V. K.; Telbiz, G. M.; Lutsenko, L. V. *Adsorpt. Sci. Technol.* **2004**, *22*, 535−541.
(11) Cowan, A. D.; Cant, N. W.; Haynes, B. S.; Nelson, P. F. *J. Catal.* **1998**, *176*, 329−343.
(12) Yan, J. Y.; Lei, G. D.; Sachtler, W. M. H.; Kung, H. H. *J. Catal.* **1996**, *161*, 43−54.
(13) Bethke, K. A.; Li, C.; Kung, M. C.; Yang, B.; Kung, H. H. *Catal. Lett.* **1995**, *31*, 287−299.
(14) Traa, Y.; Burger, B.; Weitkamp, J. *Microporous Mesoporous Mater.* **1999**, *30*, 3−41.
(15) Kwak, J. H.; Szanyi, J.; Peden, C. H. F. *Catal. Today* **2004**, *89*, 135−141.
(16) Kwak, J. H.; Szanyi, J.; Peden, C. H. F. *J. Catal.* **2003**, *220*, 291−298.
(17) Wen, B.; Yeom, Y. H.; Weitz, E.; Sachtler, W. M. H. *Appl. Catal., B* **2004**, *48*, 125−131.
(18) Chen, H. Y.; Sun, Q.; Wen, B.; Yeom, Y. H.; Weitz, E.; Sachtler, W. M. H. *Catal. Today* **2004**, *96*, 1−10.
(19) Yeom, Y. H.; Wen, B.; Sachtler, W. M. H.; Weitz, E. *J. Phys. Chem. B* **2004**, *108*, 5386−5404.
(20) Li, M. J.; Yeom, Y.; Weitz, E.; Sachtler, W. M. H. *J. Catal.* **2005**, *235*, 201−208.
(21) Yeom, Y. H.; Henao, J.; Li, M. J.; Sachtler, W. M. H.; Weitz, E. *J. Catal.* **2005**, *231*, 181−193.
(22) Li, M. J.; Yeom, Y. H.; Weitz, E.; Sachtler, W. M. H. *Catal. Lett.* **2006**, *112*, 129−132.
(23) Yeom, Y.; Li, M.; Savara, A.; Sachtler, W.; Weitz, E. *Catal. Today* **2008**, *136*, 55−63.
(24) Sung, C. Y.; Broadbelt, L. J.; Snurr, R. Q. *Catal. Today* **2008**, *136*, 64−75.
(25) Sung, C. Y.; Broadbelt, L. J.; Snurr, R. Q. *J. Phys. Chem. C* **2009**, *113*, 15643−15651.
(26) Li, H. Y.; Pu, M.; Liu, K. H.; Zhang, B. F.; Chen, B. H. *Chem. Phys. Lett.* **2005**, *404*, 384−388.
(27) Rattanasumrit, A.; Ruangpornvisuti, V. *J. Mol. Catal A: Chem.* **2005**, *239*, 68−75.
(28) McMillan, S. A.; Broadbelt, L. J.; Snurr, R. Q. *J. Catal.* **2003**, *219*, 117−125.
(29) Zygmunt, S. A.; Curtiss, L. A.; Zapol, P.; Iton, L. E. *J. Phys. Chem. B* **2000**, *104*, 1944−1949.
(30) Frash, M. V.; Kazansky, V. B.; Rigby, A. M.; van Santen, R. A. *J. Phys. Chem. B* **1998**, *102*, 2232−2238.
(31) Zheng, X. B.; Bell, A. T. *J. Phys. Chem. C* **2008**, *112*, 5043−5047.
(32) McMillan, S. A.; Broadbelt, L. J.; Snurr, R. Q. In *Environmental Catalysis*; Grassian, V., Ed.; Taylor and Francis: New York, 2005.
(33) Yeom, Y. H.; Jang, S. B.; Kim, Y.; Song, S. H.; Seff, K. *J. Phys. Chem. B* **1997**, *101*, 6914−6920.
(34) Martra, G.; Ocule, R.; Marchese, L.; Centi, G.; Coluccia, S. *Catal. Today* **2002**, *73*, 83−93.
(35) Frising, T.; Leflaive, P. *Microporous Mesoporous Mater.* **2008**, *114*, 27−63.
(36) Lowenstein, W. *Am. Mineral.* **1954**, *39*, 92−96.
(37) Ramdas, S.; Thomas, J. M.; Klinowski, J.; Fyfe, C. A.; Hartman, J. S. *Nature* **1981**, *292*, 228−230.
(38) Klinowski, J.; Ramdas, S.; Thomas, J. M.; Fyfe, C. A.; Hartman, J. S. *J. Chem. Soc., Faraday Trans. II* **1982**, *78*, 1025−1050.
(39) Barthomeuf, D. *J. Phys. Chem. B* **2005**, *109*, 2047−2054.
(40) Agarwal, V.; Conner, W. C. Jr.; Auerbach, S. M. *J. Phys. Chem. C* **2010**, *115*, 188−194.
(41) Frisch, M. J.; Trucks, G. W.; Schlegel, H. B.; Scuseria, G. E.; Robb, M. A.; Cheeseman, J. R.; Montgomery, J., J. A.; Vreven, T.; Kudin, K. N.; Burant, J. C.; Millam, J. M.; Iyengar, S. S.; Tomasi, J.; Barone, V.; Mennucci, B.; Cossi, M.; Scalmani, G.; Rega, N.; Petersson, G. A.; Nakatsuji, H.; Hada, M.; Ehara, M.; Toyota, K.; Fukuda, R.; Hasegawa, J.; Ishida, M.; Nakajima, T.; Honda, Y.; Kitao, O.; Nakai, H.; Klene, M.; Li, X.; Knox, J. E.; Hratchian, H. P.; Cross, J. B.; Bakken, V.; Adamo, C.; Jaramillo, J.; Gomperts, R.; Stratmann, R. E.; Yazyev, O.; Austin, A. J.; Cammi, R.; Pomelli, C.; Ochterski, J. W.; Ayala, P. Y.; Morokuma, K.; Voth, G. A.; Salvador, P.; Dannenberg, J. J.; Zakrzewski, V. G.; Dapprich, S.; Daniels, A. D.; Strain, M. C.; Farkas, O. M., D. K.; Rabuck, A. D.; Raghavachari, K.; Foresman, J. B.; Ortiz, J. V.; Cui, Q.; Baboul, A. G.; Clifford, S.; Cioslowski, J.; Stefanov, B. B.; Liu, G.; Liashenko, A.; Piskorz, P.; Komaromi, I.; Martin, R. L.; Fox, D. J.; Keith, T.; Al-Laham, M. A.; Peng, C. Y.; Nanayakkara, A.; Challacombe, M.; Gill, P. M. W.; Johnson, B.; Chen, W.; Wong, M. W.; Gonzalez, C.; and Pople, J. A. *Gaussian 03*, revision D.02 ed.; Gaussian, Inc.: Wallingford, CT, 2004.
(42) McQuarrie, D. A. *Statistical Mechanics*, 1st ed.; University Science Books: Sausalito, CA, 2000.
(43) McMillan, S. A.; Broadbelt, L. J.; Snurr, R. Q. *J. Phys. Chem. B* **2002**, *106*, 10864−10872.
(44) Vanduijneveldt, F. B.; Vanduijneveldtvanderijdt, J. G. C. M.; Vanlenthe, J. H. *Chem. Rev.* **1994**, *94*, 1873−1885.
(45) Hansen, N.; Brueggemann, T.; Bell, A. T.; Keil, F. J. *J. Phys. Chem. C* **2008**, *112*, 15402−15411.
(46) Swisher, J. A.; Hansen, N.; Maesen, T.; Keil, F. J.; Smit, B.; Bell, A. T. *J. Phys. Chem. C* **2010**, *114*, 10229−10239.
(47) De Moor, B. A.; Reyniers, M. F.; Sierka, M.; Sauer, J.; Marin, G. B. *J. Phys. Chem. C* **2008**, *112*, 11796−11812.
(48) Viswanathan, U.; Fermann, J. T.; Toy, L. K.; Auerbach, S. M.; Vreven, T.; Frisch, M. J. *J. Phys. Chem. C* **2007**, *111*, 18341−18347.
(49) Koranyi, T. I.; Nagy, J. B. *J. Phys. Chem. C* **2007**, *111*, 2520−2524.
(50) Peterson, B. K. *J. Phys. Chem. B* **1999**, *103*, 3145−3150.